HHS Public Access

Author manuscript

Neuron. Author manuscript; available in PMC 2019 January 17.

Published in final edited form as:

Neuron. 2018 January 17; 97(2): 356–367.e4. doi:10.1016/j.neuron.2017.12.027.

Integration of plasticity mechanisms within a single sensory neuron of *C. elegans* actuates a memory

Josh D. Hawk[1], **Ana C. Calvo**[1], **Ping Liu**[2], **Agustin Almoril-Porras**[1], **Ahmad Aljobeh**[1], **María Luisa Torruella-Suárez**[1], **Ivy Ren**[1], **Nathan Cook**[1], **Joel Greenwood**[1,3], **Linjiao Luo**[4], **Zhao-Wen Wang**[2], **Aravinthan D.T. Samuel**[3], and **Daniel A. Colón-Ramos**[1,5,6]

[1]Program in Cellular Neuroscience, Neurodegeneration and Repair, Department of Cell Biology and Department of Neuroscience, Yale University School of Medicine, P.O. Box 9812, New Haven, CT, 06536-0812, USA

[2]Department of Neuroscience, University of Connecticut Health Center, Farmington, Connecticut 06030, USA

[3]Department of Physics and Center for Brain Science, Harvard University, Cambridge, MA 02138

[4]Key Laboratory of Modern Acoustics, Ministry of Education, Department of Physics, Nanjing University, Nanjing 210093, China

[5]Instituto de Neurobiología, Recinto de Ciencias Médicas, Universidad de Puerto Rico, 201 Blvd del Valle, San Juan, Puerto Rico

Summary

Neural plasticity—the ability of neurons to change their properties in response to experiences—underpins the nervous system's capacity to form memories and actuate behaviors. How different plasticity mechanisms act together *in vivo* and at a cellular level to transform sensory information into behavior is not well understood. We show that in *Caenorhabditis elegans* two plasticity mechanisms—sensory adaptation and presynaptic plasticity—act within a single cell to encode thermosensory information and actuate a temperature-preference memory. Sensory adaptation adjusts the temperature range of the sensory neuron (called AFD) to optimize detection of temperature fluctuations associated with migration. Presynaptic plasticity in AFD is regulated by the conserved kinase nPKCε and transforms thermosensory information into a behavioral preference. Bypassing AFD presynaptic plasticity predictably changes the learned behavioral preferences without affecting sensory responses. Our findings indicate that two distinct

[6]Corresponding Author and Lead Contact: Daniel A. Colón-Ramos, Ph.D. Department of Cell Biology, Department of Neuroscience, Yale Program in Cellular Neuroscience, Neurodegeneration and Repair, Yale University School of Medicine, 333 Cedar St, SHM B163D, New Haven, CT 06510, daniel.colon-ramos@yale.edu.

Author Contributions. J.D.H and D.A.C.-R. designed experiments. J.D.H., A.C.C, P.L., A.A.-P, A.A., M.L.T.S, I.R., and N.C. performed experiments and data analyses. J.D.H., A.C.C., A.A.-P, A.A., M.L.T.S, N.C., L.L. and J.G. developed reagents and protocols. J.D.H., A.D.T.S, Z.-W.W and D.A.C.-R. prepared the manuscript.

Declaration of Interests. The authors declare no competing interests.

neuroplasticity mechanisms function together through a single-cell logic system to enact thermotactic behavior.

eTOC

Neural plasticity—the ability of neurons to change their cellular properties in response to past experiences—underpins memory. Hawk et al. show that in *C. elegans* a single-cell logic system can both represent sensory stimuli and guide memory-based behavioral preference.

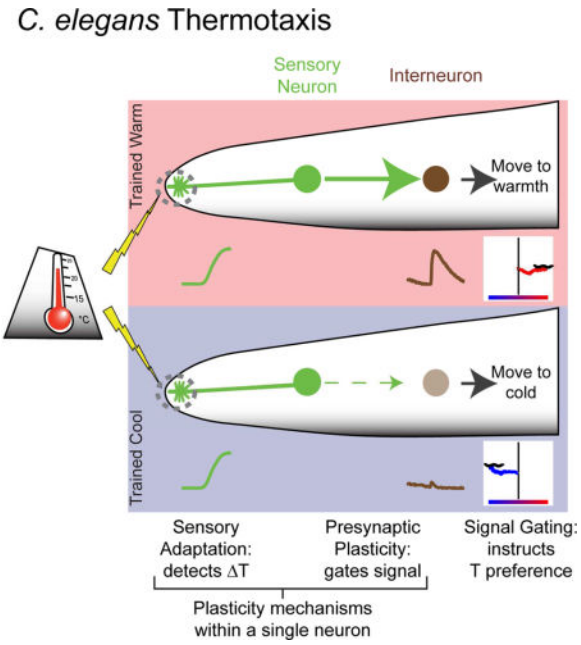

Introduction

When an animal experiences a favorable condition, it can form a memory that guides its future behavior. The future performance of these learned behavioral preferences requires the animal to navigate sensory-rich environments, extract behaviorally-relevant information and differentially act based on its previous experience. While it is widely accepted that plasticity mechanisms underpin experience-driven behaviors, how different plasticity mechanisms act *in vivo* and within single cells to facilitate recall and actuation of learned behavioral preferences is not well understood (Basu and Siegelbaum, 2015; Davis, 2011; Gjorgjieva et al., 2016; Mayford et al., 2012).

The nematode *C. elegans* does not have an innate preferred temperature. Instead, *C. elegans* cultivated at a given temperature will remember this temperature (T_C) and migrate towards it when on a thermal gradient (Hedgecock and Russell, 1975). This memory can be trained to a new temperature within four hours (Biron et al., 2006; Chi et al., 2007; Hedgecock and Russell, 1975; Mohri et al., 2005; Ramot et al., 2008b) (Figure 1B–D). Neurons specifically required for thermotaxis behavior have been identified by neuronal ablation studies (Beverly et al., 2011; Biron et al., 2008; Kuhara et al., 2008; Mori and Ohshima, 1995), and their connectivity is known (White et al., 1986). From this work, we understand that temperature

preference depends on a thermosensory neuron, called AFD, which has specialized molecular pathways that allow it to respond to temperature changes as small as 0.1°C (Clark et al., 2006; Kimura et al., 2004; Mori and Ohshima, 1995; Ramot et al., 2008a). AFD responses are observed only near an adaptable sensory threshold that correlates, on long timescales, with the cultivation temperature memory. These observations led to the hypothesis that the AFD thermosensory threshold represents the memory for the preferred temperature (Aoki and Mori, 2015; Biron et al., 2006; Garrity et al., 2010; Kimura et al., 2004; Luo et al., 2014; Yu et al., 2014). AFD has also been observed to adapt its thermosensory threshold on short timescales (Ramot et al., 2008a; Yu et al., 2014), but the behavioral repercussions of this more rapid adaptation have not been examined. Thus, the role of the adaptable AFD sensory threshold in the actuation of the cultivation temperature memory is not well understood.

Results

To better understand AFD sensory responses in relationship to thermotaxis behavior, we developed a custom thermoelectric control system (see Materials and Methods and Figure S1A) that can rapidly (~1°C/second) and precisely (+/− 0.02°C) control temperature while we image calcium dynamics using GCaMP6 (Chen et al., 2013) in individual neurons of live animals. Implementing similar conditions to those used in published studies, we reproduced the observation that sensory thresholds in AFD correlate with the cultivation temperature memory when tested immediately after training (Figure 1E and Figure S1B–E). To examine whether the AFD response threshold persists long enough to store behavioral memory, animals trained at 15°C, 20°C or 25°C (T_C) were subsequently held for 30 minutes at 20°C (T_H) (Figure 1A). We observed that when the cultivation temperature memory (T_C) differed from just-experienced holding temperatures (T_H), AFD sensory threshold responses adapted to the new holding temperature (Figure 1I), although animals still performed according to the cultivation temperature memory (Figure 1F–H). Thus, experience on a short timescale, represented by T_H, controls the threshold of AFD sensory responses, whereas the behavioral preference is regulated on a longer timescale of hours to set the cultivation temperature memory, T_C. While our findings are consistent with reports that behavioral memory persists for hours (Biron et al., 2006; Chi et al., 2007; Hedgecock and Russell, 1975; Mohri et al., 2005; Ramot et al., 2008b) and that AFD adaptation occurs in minutes (Ramot et al., 2008a; Yu et al., 2014), our findings are inconsistent with the hypothesis that the cultivation temperature memory resides in the AFD thermosensory thresholds. Instead, our findings suggest that the sensory threshold in AFD represents the holding temperature the animal has recently experienced.

How fast are AFD sensory thresholds adapting to newly experienced temperatures? We observed that AFD adapted to the holding temperature within minutes (Figure 1J & Figure S2U–W) consistent with previous reports (Ramot et al., 2008a; Yu et al., 2014). AFD adaptation kinetics were mostly (>90%) complete within two minutes to increasing temperatures, and within thirty minutes to decreasing temperatures (Figure 1J). Analyses of AFD thermosensory response kinetics with distinct thermal stimuli (Figure S2A–L) and differing holding temperatures (Figure S2M–T) further demonstrate that AFD responds to increases in temperature above the just-experienced ambient temperature (i.e., the holding

temperature) without reference to the absolute temperature or the behaviorally preferred temperature (i.e., the cultivation temperature). Because increased calcium buffering can slow the rate of AFD adaptation (Ramot et al., 2008a) and genetically encoded calcium indicators can act as calcium buffers (Miyawaki et al., 1999), it is possible that the true rate of adaptation is even faster than that observed in this study or previous work (Ramot et al., 2008a; Yu et al., 2014). Consistent with a role of AFD sensory response supporting migration rather than storing preference, kinematic analyses of thermotaxis behavior indicate that animals continue to migrate towards their preferred cultivation temperature (T_C) well after the AFD responses have adapted to T_H (Figure 1J,K), underscoring that the sensory threshold responses of AFD are separable from the cultivation temperature memory.

If the sensory thresholds in AFD are not the cultivation temperature memory, what do these sensory responses represent? Our findings indicate that the AFD thermosensory neuron detects temperature fluctuations from the recently-experienced ambient temperature (Figure 1 and Figure S2). The fast kinetics of adaptation allows AFD to maintain sensitivity to temperature changes while migrating in a gradient. This interpretation of the AFD thermosensory responses is consistent with observed kinetics of adaptation in calcium imaging (Yu et al., 2014) (Figure 1J and Figure S2U–W) and electrophysiological studies (Ramot et al., 2008a) performed in AFD.

We also note that this interpretation of AFD function, and the kinetics of AFD adaptation, helps explain and unify previous observations in the field. For example, when animals are first placed at 20°C in a temperature gradient, a consistent delay of at least 15 minutes prior to thermotaxis performance is observed for animals trained at 23°C (T_C), but is not observed for animals trained at 17°C (T_C) (Ito et al., 2006), also (Figure 1K). Our model predicts this asymmetric delay in the initiation of thermotaxis behavior based solely on the asymmetric kinetics of AFD adaptation (Figure 1J). The AFD adaptation kinetics also allowed us to predict and model AFD thresholds during behavioral performance (Figure S2X, dashed lines), highlighting that adaptation occurs prior to movement of the animals in the thermotaxis gradients (Figure S2X, solid lines). Together our findings indicate that fast sensory adaptation allows AFD to remain sensitive to local temperature variations. By encoding thermosensory information as changes in temperature (Clark et al., 2006; Kimura et al., 2004) and by quickly adapting its sensory thresholds (Ramot et al., 2008a; Yu et al., 2014), AFD serves as an adaptable “compass”, indicating to the animal its bearing as it navigates temperature gradients.

Next, we examined how AFD transfers thermal information onto its only chemical postsynaptic partner, AIY (White et al., 1986). We observed various temperature-dependent dynamics in AIY, some which were independent of thermosensory neuron AFD (Figure S3). This indicates that not all temperature responses in AIY are AFD-dependent and that other, AFD-independent mechanisms of temperature sensation exist and converge at AIY, consistent with (Beverly et al., 2011; Biron et al., 2008; Kuhara et al., 2008) (see also AWC-dependent responses in Figure S3I). Importantly, our analyses revealed one thermally evoked positive calcium transient that was dependent on AFD: a response to warming near holding temperature (Clark et al., 2006) (Figure 2E, F and Figure S3). Consistent with this dependence, we observed that this AIY response to warming is similar in terms of timing to

the responses seen in AFD (Figure 2A, G). However, the frequency of animals displaying responses in AIY is lower than the frequency of animals displaying responses in AFD (Figure 2A vs 2E).

To better understand the relationship between the responses in AFD and the responses in AIY, we examined animals expressing GCaMP6 in AFD or AIY at varying cultivation temperatures (Figure 2, Figure S4A–F, and Figure S4O). We observed that while warming above the holding temperature (20°C for Figure 2) reliably elicits responses in AFD regardless of T_C experience, the frequency of warming responses in AIY depends, not on absolute temperature preferences, but on the relationship between T_H and T_C (Figure 2B vs H, Figure S4A–F, and Figure S4O). For example, when T_H=T_C, response frequency in AIY is ~50% and this frequency is irrespective of the absolute values of the temperatures (Figure 2H and Figure S4O). Similarly, in conditions in which T_H>T_C, regardless of what those absolute temperature values are, wild type animals perform negative thermotaxis (i.e., move towards colder temperatures), and AIY responses are infrequent (Figure 2H: 27/75 animals, ~36%). In conditions in which T_H<T_C, in which wild type animals perform positive thermotaxis (i.e., move towards warmer temperatures), AIY responses were frequent (Figure 2H: 44/65, ~68%). To examine whether the observed changes in AIY response frequency follow a time course similar to the change in behavioral memory, we re-trained animals from T_H>T_C to T_H<T_C (and vice versa) with variable durations of re-training (Figure 2K–L). We found that the kinetics of AIY re-training were similar to the observed timecourse for behavioral memory retraining ((Hedgecock and Russell, 1975) and Fig 2K–L). Our findings indicate that cultivation temperature experience affects AIY responses to AFD signaling in a way that correlates with the temperature preference of the animal.

To understand how temperature preference is represented in the AIY responses, we examined mutants that affect temperature preference behaviors. Mutations that impair PKC-1 function do not affect AFD sensory responses (Luo et al., 2014) (Figure 3D–G and Figure S4G–N), yet produce robust thermotaxis behavioral defects (Okochi et al., 2005) (Figure 3A–C). PKC-1 loss-of-function mutants perform experience-independent positive thermotaxis, while expression of a constitutively active form of PKC-1 cell-specifically in AFD (*pAFD::caPKC-1*) produces experience-independent negative thermotaxis (Figure 3A–C). Defects observed with PKC-1 loss-of-function can be rescued by expression of wild-type PKC-1 in AFD alone (Okochi et al., 2005). Thus, both positive and negative thermotaxis behaviors are dependent on PKC-1 activity specifically in AFD.

When we examined temperature-dependent calcium responses in AIY in these genetic backgrounds, we observed that in worms expressing *pAFD::caPKC-1*, which perform experience-independent negative thermotaxis (Figure 3A), the frequency of the warming-evoked response in AIY is diminished as compared to wild type in similar conditions (Figure 3I, Figure S4H, J). This genetic manipulation phenocopies the change in AIY calcium responses observed for wild type animals trained to perform negative thermotaxis (Figure S4H vs B). Conversely, in the *pkc-1* loss-of-function mutants, which perform experience-independent positive thermotaxis (Figure 3C), warming response frequency in AIY increases relative to *pAFD::caPKC-1* and wild-type worms in similar conditions (Figure 3I and Figure S4H,J,L), but phenocopies wild type animals trained to perform

positive thermotaxis (Figure S4F). Our findings indicate that AIY thermal responses in *pkc-1* gain-of-function and loss-of-function mutant animals phenocopy those seen for wild-type animals trained to perform negative or positive thermotaxis, respectively. Our data suggest that AIY response fidelity within a population is predictive of the temperature preference behavior. Our findings are consistent with previous studies that indicated that AFD synaptic output can be modulated independently of AFD sensory adaptation (Biron et al., 2006), and indicate that PKC-1 activity in AFD governs thermotaxis behavior, not by modulating AFD sensory responses, but by altering AFD to AIY communication.

To understand how AFD to AIY communication could be modulated to encode a temperature preference, we performed whole-cell patch clamp electrophysiology on AIYs of wild-type, *pkc-1* gain-of-function, and loss-of-function mutant animals cultivated at (Figure 4). *C. elegans* interneurons have high membrane resistances (AIY resistance is 4–8 GΩ (Narayan et al., 2011)), therefore small spontaneous post-synaptic currents (sPSC) are predicted to have substantial implications for membrane potential. To reliably detect these small sPSC in AIY while manipulating temperature, we adapted an electrophysiological protocol previously used to measure temperature responses in AFD (Ramot et al., 2008a) and used a high chloride pipette recording solution (see **Methods**). Our recording conditions do not differentiate excitatory versus inhibitory inputs, but provide stable and sensitive detection of small sPSC.

We subjected animals to sequential warming and cooling thermal ramps (which depolarize and hyperpolarize AFD, respectively (Ramot et al., 2008a)) from a holding temperature similar to the cultivation temperature (20°C). We predicted that the frequency of sPSCs in AIY would be increased during the warming ramp due to membrane depolarization-induced neurotransmitter release from AFD. Indeed, in both wild-type and PKC-1 gain-of-function animals, AIY often displayed an increase in sPSC frequency near the AFD threshold temperature (20°C) during the warming ramp (Figure 4A, black arrowhead). The frequency of sPSCs during the warming ramp in AFD-specific PKC-1 gain-of-function animals was significantly higher (55.4 +/−17.3 events/min, n=8) than that in *pkc-1* loss-of-function animals (10.9 +/−4.4 events/min, n=10), with intermediate frequency in wild-type animals (21.7 +/− 5.6 events/min, n=13) (Figure 4B). Neither the averaged shape nor the mean amplitude of sPSCs during the warming ramp was different between the genotypes (Figure 4C: GOF 3.10+/−0.24 pA; WT 2.71+/−0.18 pA; LOF 3.01+/−0.40 pA). In contrast, cooling did not produce a clear temperature-locked pattern of activity in any of the examined genotypes (Figure 4D). Furthermore, there were no significant effects of *pkc-1* genotype on sPSC rate during the cooling stimulus (Figure 4E: GOF 11.3 +/−3.7 events/min, n=8; WT 10.5 +/−2.5 events/min, n=13; LOF 12+/−5.7 events/min, n=10). Because differences in baseline sPSC frequency among worms within each group may overshadow the effect of warming, we also calculated the difference between sPSC frequency during warming and cooling periods in each animal and compared these normalized sPSC rates among the three genotypes. This analysis revealed statistically significant differences among all the three genotypes with the rate of sPSCs proportional to the expected activity of PKC-1 (Fig 4F: GOF cooling +44.1 +/−14.2 events/min; WT cooling +10.5 +/−3.7 events/min; LOF cooling −1.1 +/−3.1 events/min).

Previous studies have indicated that PKC-1 facilitates presynaptic release in *C. elegans* neurons (Sieburth et al., 2007; Ventimiglia and Bargmann, 2017) and its mammalian homologue nPKCε has been implicated in presynaptic plasticity in mammalian hippocampal neurons (Son et al., 1996; Zisopoulou et al., 2013). Our electrophysiological results are consistent with these studies and indicate that PKC-1 activity within AFD facilitates neurotransmitter release onto AIY to alters its thermal responses. Importantly, our findings indicate that PKC-1 regulates thermal preference by modulating presynaptic plasticity at the AFD to AIY synapse.

Our findings also support a model in which a synaptic gate from AFD to AIY determines the temperature preference and instructs whether worms move up or down the gradient towards their previously learned preferred temperature. AFD responses to temperature do not vary based on the temperature preference of the animal. But in animals that prefer warmer temperatures (or in animals lacking PKC-1), when AFD responds to increases in temperature there is a higher probability that those responses will be transduced to AIY. That increased probability of responses in AIY instructs positive thermotaxis. Conversely, in animals that prefer colder temperatures (or in animals with a PKC-1 gain-of-function in AFD), while AFD responds similarly to animals reared at warmer temperatures, there is a lower probability that those responses will be transduced to AIY. This “closed” synaptic gate is necessary to permit negative thermotaxis. Because we did not observe an impact of training temperature on calcium response amplitude in the presynaptic region (Figure S1B), we suspect that the mechanism controlling synaptic output is downstream of axonal calcium influx. Our results and model are also consistent with the long known effect of AIY inactivation on thermotaxis, which results in constitutively negative thermotaxis regardless of previous experience (Biron et al., 2006; Hobert et al., 1997; Kuhara et al., 2011; Luo et al., 2014; Mori and Ohshima, 1995).

If our core behavioral model is correct, and expression of the cultivation temperature memory depends on regulation of synaptic communication between AFD and AIY, then directly coupling AIY activity to AFD would make animals perform positive thermotaxis regardless of previous experience. To test this prediction, we heterologously expressed the mammalian gap junction protein connexin 36 (CX36) (Rabinowitch et al., 2014). Invertebrate organisms do not endogenously express connexins, and mammalian connexins do not interact with endogenous invertebrate innexins to form synthetic gap junctions (see (Epstein and Gilula, 1977; Rabinowitch et al., 2014) and **Methods**). Consistent with this, expression of CX36 in either AFD or in AIY alone did not impact thermotaxis behavior (Figure S5A, B). Expression of CX36 in both AIY and AFD, however, should result in an ectopic gap junction between both neurons. Indeed, simultaneous expression of CX36 in AFD and AIY (*AFD/AIY::CX36*) changed the thermal response profile of AIY to match that of AFD (Figure S5I–K). Our findings suggest that simultaneous expression of CX36 in AFD and AIY results in a synthetic gap junction that electrically couples the responses of these two neurons.

We observed that expression of connexin channels in both AFD and AIY enhanced AFD-elicited AIY responses (Figure 5A, B) without altering AFD thermosensory response threshold, frequency or kinetics (Figure S5C–E, H–K). Specifically, we observed that

animals trained to perform negative thermotaxis (T_H>T_C) displayed enhanced thermosensory response frequency in AIY when expressing the synthetic AFD:AIY gap junction (Figure 5A, B). Consistent with the model in which AFD to AIY connectivity drives behavioral outcome, these animals with the synthetic electrical synapses perform positive thermotaxis (Figure 5D) despite an experience history (T_H>T_C) that promotes negative thermotaxis (Figure 5C). These findings indicate that the synthetic electrical synapse bypasses endogenous plasticity of the AFD-AIY chemical synapse to recode the behavioral preference.

We then examined whether the synthetic gap junction could bypass regulation of AFD-AIY plasticity by PKC-1. Consistent with our model, we observed that attenuation of AIY responses seen in the *pAFD::caPKC-1* animals (Figure 5E) is suppressed by expression of the synthetic AFD:AIY gap junction (Figure 5F). Moreover, the synthetic AFD:AIY gap junction was sufficient to convert negative thermotaxis observed in *pAFD::caPKC-1* mutants (Figure 5G) into positive thermotaxis (Figure 5H). Our findings indicate that modulation of the AFD:AIY synapse governs expression of the cultivation temperature memory.

Discussion

The present work reconciles the observed fast timescale of AFD sensory adaptation with the hours-long behavioral memory and suggests that sensory adaptation and presynaptic plasticity, two distinct plasticity modules, act cell-autonomously in AFD to actuate thermotaxis behavior. Our findings are also consistent with recent studies on AFD responses in freely moving animals, which demonstrate that AFD activities contain enough information to represent the thermal environment (Tsukada et al., 2016). Our findings extend those observations and demonstrate that AFD sensory responses are not dependent on the cultivation temperature memory, nor do they represent absolute temperatures (Clark et al., 2006; Kimura et al., 2004; Ramot et al., 2008a). Instead, AFD responds to changes from the current temperature. We propose that AFD sensory responses act, metaphorically speaking, as an “adaptable compass”, making themselves most sensitive to the local temperature environment to detect gradients. Together with electrophysiological studies (Ramot et al., 2008a), our findings suggest that warming and cooling might activate and inactivate AFD, respectively, allowing the temperature-evoked pattern of AFD activity to encode the direction of a worm’s movement in a temperature gradient.

The fast kinetics of AFD sensory adaption are likely to be important for maintaining perceptual constancy in a dynamic and sensory-rich environment. One of the better understood sensory adaptation systems is the vertebrate photoreceptor, which act as a contrast detector over wide dynamic ranges of illumination (Fain et al., 2001). Sensory adaptability in photoreceptor cells depends on a conserved mechanism that includes Guanylate Cyclases (GCs), Guanylate Cyclases Activating Protein (GCAP) and cGMP (Fesenko et al., 1985; Yau and Nakatani, 1985). Interestingly, molecular genetic studies in AFD have identified cGMP-dependent mechanism as necessary for temperature sensing (Inada et al., 2006; Komatsu et al., 1996; Ramot et al., 2008a; Wang et al., 2013), and recent studies in vertebrates and *C. elegans* suggest that guanylate cyclases respond to temperature (Chao et al., 2015; Takeishi et al., 2016). Our findings extend these studies, now

demonstrating that sensory adaptation in AFD is important for thermotaxis behavior by enabling the animal to maintain contrast sensitivity and perceptual constancy over wide environmental variation.

Modulation of temperature preference is actuated by PKC-1, which is required cell-autonomously in the presynaptic AFD neuron. In other *C. elegans* neuron, PKC-1 facilitates presynaptic release (Sieburth et al., 2007; Ventimiglia and Bargmann, 2017). The vertebrate homologue of PKC-1, called nPKCε, is a conserved molecule which has been implicated in presynaptic plasticity in the mammalian hippocampus and in memory (Son et al., 1996; Zisopoulou et al., 2013). Consistent with PKC-1 modulating presynaptic plasticity in AFD to instruct temperature preference, we find from our electrophysiological studies that PKC-1 facilitates neurotransmission. PKC-1 is modulated by DAG, and a DAG regulator *dgk-3* has been shown to act cell-autonomously in AFD to control temperature preference and alter AIY threshold adaptation parameters without affecting AFD thermosensory responses (Biron et al., 2006). Based on our studies and published findings, we propose that an nPKCε-dependent presynaptic plasticity mechanism acts in AFD to actuate the temperature preference memory through the control of an AFD to AIY synaptic gate, where the flow of a positively coupled AFD to AIY signal is throttled to control direction of travel on a thermal gradient.

The neurotransmitter logic of AFD is likely important in regulating AIY responses and expressivity of the temperature preference. While the neurotransmitter logic between AFD and AIY, and how it contributes to thermotaxis behavior, is not fully understood there is evidence that AFD can transmit excitatory (Clark et al., 2006; Narayan et al., 2011) and inhibitory (Ohnishi et al., 2011) signals onto AIY. Our electrophysiological data indicate that PKC-1 facilitates neurotransmission, while our calcium imaging data indicate that PKC-1 silences AIY. Our studies are consistent with the model that AFD has both excitatory and inhibitory mechanisms of neurotransmission onto AIY, and suggest that the balance between these AFD-derived excitatory and inhibitory signals (Kuhara et al., 2011), likely regulated by PKC-1 mediated presynaptic plasticity, contributes to the direction of migration in thermotaxis behavior.

The state of the AFD-AIY synaptic gate encodes whether AFD-derived thermosensory information will be interpreted as attractive or repulsive. On temperature gradients, AFD responds to increases in temperature regardless of the cultivation temperature memory. Positive thermotaxis occurs when these AFD responses are transmitted onto AIY, while negative thermotaxis occurs when these AFD responses fail to activate AIY. While we do not yet understand the downstream circuits differentially activated by AIY to instruct goal-oriented locomotion, our model reconciles with the known role of AIY in suppressing turns during *C. elegans* locomotion (Gray et al., 2005; Kocabas et al., 2012; Li et al., 2014). For instance, the dynamic coupling of a warming signal to AIY would be expected to yield positive thermotaxis by suppressing turns selectively when the animal is migrating up a gradient. In this way, the integration of two plasticity mechanisms in AFD and selective activation of AIY based on previous experience could instruct movement towards a preferred temperature.

In this study, we have examined orthothermal thermotaxis (movement up or down the gradient), which, under physiological conditions, brings the animal to the proximity of their preferred temperature. It has been reported (and we also observe) that upon reaching a preferred temperature, animals switch from orthothermal movement to isothermal tracking (moving within 0.1C of their preferred temperature) (Hedgecock and Russell, 1975; Luo et al., 2006; Ryu and Samuel, 2002). Interestingly, in the *pkc-1* mutants or the AFD/AIY::CX36 coupled strain, animals never reach a "preferred" temperature or perform isothermal behavior. Instead, we observe a persistent and abnormal drive in a particular direction on the gradient. Our findings are consistent with previous studies that demonstrate that isothermal and orthothermal movement are two distinct and genetically separable behaviors (Colosimo et al., 2004; Ryu and Samuel, 2002), and suggest that mechanisms modulated by PKC-1 encodes for direction of migration rather than 'storing' the memory for a preferred temperature.

Actuation of a learned preference behavior requires perceptual constancy during navigation of the sensory rich environments and the flexibility to differentially respond to sensory stimuli based on previous experiences. In this work, we have found that a two component system in a single sensory neuron is capable of encoding sensory-rich information, maintaining perceptual constancy, and flexibly assigning value based on memory. Bipartite plasticity through adaptation and synaptic mechanisms has been observed in at least one other *C. elegans* sensory neuron (Cho et al., 2016) and in *Drosophila*, where starvation produces complementary presynaptic facilitation and inhibition of sensory transmission to drive appetitive behavior (Ko et al., 2015; Root et al., 2011). Together, these findings suggest that the logical architecture composed of a directional sensory signal, integrated with a preference signal at the synapse, may be a common feature within sensory physiology. Therefore, integration of plasticity modules, in the case of *C. elegans* thermotaxis within a single neuron, can cooperatively transform sensory information into a behavioral decision to actuate learned behavioral preference.

STAR Methods Section

CONTACT FOR REAGENT AND RESOURCE SHARING

Further information and requests for resources and reagents should be directed to and will be fulfilled by the Lead Contact Daniel Colón-Ramos (daniel.colon-ramos@yale.edu).

EXPERIMENTAL MODEL AND SUBJECT DETAILS

Worms were cultivated at 20°C on nematode growth medium seeded with a lawn of *Escherichia coli* strain OP50 using standard methods (Brenner, 1974). Young adult hermaphrodites were used for all experiments. The strains used in this study are listed in the Key Resources Table.

METHOD DETAILS

Thermotaxis Behavioral Assay—Animals were reared at 20°C for all experiments with shifts to the training temperature 4 hour prior testing. High-throughput behavioral analyses were performed as described (Luo et al., 2014). Briefly, synchronized young adult

populations were washed in M9 (Stiernagle, 2006), then transferred by pipette to the 20°C isotherm of the behavioral test plate (22-cm × 22-cm agar plates with 18°C to 22°C thermal gradient). Migration was monitored for >30 min at 2fps using a MightEx camera (BCE-B050-U). Trajectories were analyzed using an adaptation of the MagatAnalyzer software package as previously described (Gershow et al., 2012; Luo et al., 2014).

Molecular Biology and transgenic lines—Gateway recombination (Invitrogen) was used to generate *C. elegans* expression plasmids for caPKC-1, GCaMP6, caspases and CX36. For PCR-based cloning and subcloning of components into the Gateway system, either Phusion or Q5 High-Fidelity DNA-polymerase (NEB) was used for amplification. All components were sequenced within the respective Gateway entry vector prior to combining components into expression plasmids via a four-component Gateway system (Merritt and Seydoux, 2010). For production of the caPKC-1 transgene, wild-type *pkc-1* cDNA was isolated from a mixed stage *C. elegans* cDNA library using primers amplifying transcript *F57F5.5b* and overhangs that allowed subsequent recombination into the vector pDONR221 (Invitrogen). The pseudosubstrate domain mutation (A160E) (Okochi et al., 2005) was introduced using QuikChange mutagenesis (Stratagene). GCaMP6s, cz::caspase-3(p17), caspase-3(p12)::nz, and CX36 were introduced into pDONR221 using a similar PCR-based strategy from plasmid sources (Chelur and Chalfie, 2007; Chen et al., 2013; Rabinowitch et al., 2014). Cell-specific promoters were introduced using the pENTR 5′-TOPO vector (Invitrogen) after amplification from genomic DNA or precursor plasmids. Transgenic lines were created by microinjection into the distal gonad syncytium (Mello and Fire, 1995) and selected based on expression of one or more co-injection markers: *Punc-122::GFP, Punc-122::dsRed, Pelt-7::GFP::NLS, Pelt-7::mCherry::NLS, or Pmyo-3::mCherry*. In those cases where extrachromosomal arrays were integrated, incorporation into the genome was induced with trimethylpsoralen (TMP) activated by UV using standard procedures followed by outcross. All integrated lines were outcrossed at least four times before testing.

Calcium Imaging—For imaging, worms were mounted on a thin pad of 5% agarose in M9 buffer between two standard microscope coverslips. Worms were immobilized with 7.5–10mM levamisol (Sigma). All solutions were pre-equilibrated to the holding temperature prior to sample preparation. Prepared coverslip assemblies were placed at T_H on the peltier surface of the thermoelectric control system as illustrated in Figure S1a. A thermal probe (SRTD-2, Omega) mounted onto the surface of the peltier was used for feedback control via a commercially available proportional-integral-derivative (PID) controller (FTC200, Accuthermo). Target temperatures were supplied to the PID controller by a custom computer interface written in LabView (National Instruments), which subsequently gated current flow from a 12V power supply to the peltier via an H-bridge amplifier (FTX700D, Accuthermo). Excess heat was removed from the peltier with a water cooling system. Precise temperature control was initially confirmed with an independent T-type thermal probe (IT-24P, Physitemp) attached to a hand-held thermometer (HH66U, Omega) and routinely compared to incubator temperatures with an infrared temperature probe (Actron). After mounting worms and placing them on the thermal control stage, fluorescence time-lapse imaging was begun immediately prior to implementing the temperature protocol in LabView, and temperature readings were recorded continuously while imaging. Fluorescence time-lapse

imaging (250ms exposure) was performed using a Leica DM5500 microscope with a 10X/0.40 HC PL APO air objective. A Photometrics Dual-View 2 (DV2) optical splitter was used to simultaneously project distinct green and red fluorescence images onto the two halves of a Hamamatsu ORCA-Flash4.0 LT camera. Image acquisition, segmentation into regions of interest, and color alignment were performed in MetaMorph (Molecular Devices). Downstream data processing was performed using custom scripts written in MATLAB (Mathworks), including alignment of fluorescence intensity values to the temperature stimulus, ratiometric signal analyses, calcium response detection, and initial figure production. Temperature readings were assigned to image frames in MATLAB based on CPU timestamps on images and temperature readings. We employed best practices in acquisition and analyses of calcium imaging data in live animals, including the use of stably integrated transgenic lines with wild type thermotaxis behaviors, robust analyses of large number of animals and blind scoring of phenotypes (Broussard et al., 2014; Chen et al., 2013; Tian et al., 2012). Our calcium imaging strain and microscope optical design allow ratiometric analyses comparing GCaMP6 green fluorescence to signal from a calcium-independent red fluorophore, mCherry or tagRFP. Comparing our analysis using ratiometric normalization with analysis using the green channel alone, we observed indistinguishable patterns of activity. Because of this observation and because some subsequently used markers (e.g. *Pmyo-3::mCherry* strains) produce additional red fluorescent signal in the head that can alter ratio baselines, we report fluorescence for the green channel alone. Our initial analysis of AFD response to changes from the holding temperature (Figure S2A–L) showed us that AFD adapts rapidly, an effect that we confirmed with detail kinetic analysis of AFD adaptation rate (Figure 1J). Because of these rapid adaptation kinetics, we minimized the total duration of our stimulus protocols to reduce the impact of adaptation on AFD threshold measurements. Also, we observed that ramping rate did not impact calcium dynamics (Figure S2B,F,J). The lack of relationship between AFD calcium rise and ramp rate in our study suggests that the impact of thermal gradient steepness on behavioral performance (Beverly et al., 2011; Ramot et al., 2008b) may be a consequence of other circuit inputs. For these reasons, we used a rapid ramping rate (1°C/10sec) to assess AFD response threshold accurately. Response thresholds were determined with both computer-assisted response selection by a blind human observer and an automated script utilizing signal intensity and its derivative; these two methods showed high concordance. These methods determined the AFD and AIY response threshold as the initial rise of the calcium response for all experiments. Heat map scaling, response graphing, and response detection thresholds were performed with the same consistent settings within each experiment. Heat maps were displayed using the Matlab ‘imagesc’ function, which scales data to the full color range available. The same scaling was applied to all comparable data within a figure. Unless otherwise specified, the scaling was based upon the highest intensity data set to minimize saturation. For analyses of AFD calcium signals, we selected four regions of interest: sensory ending, soma, axon, and a control region outside of AFD. We observed similar response profiles for all three regions within AFD, consistent with previous reports (Clark et al., 2006) and quantified in Figure S1B. Because the sensory ending is isolated from other sources of fluorescence (such as autofluorescence) and is the identified origin of thermosensory signals (Clark et al., 2006), the reported responses in our manuscript are at the sensory endings. Comparisons of signals in the axon and sensory ending of AFD show

high concordance with no differential impact of training condition (Figure S1). For analyses of AIY, we divided the neuron into four previously defined and morphologically distinct regions based on EM reconstruction micrographs (White et al., 1986), as described (Colon-Ramos et al., 2007): 1) soma; 2) an asynaptic zone proximal to the soma (Zone 1); 3) a synapse-rich ~5uM long region in which the neurite turns dorsally from the anterior ventral nerve cord into the nerve ring (Zone 2); and 4) a distal segment within the nerve ring with sparse presynaptic distribution (Zone 3). In our analyses, we quantified signal intensity in the AIY soma and synaptic Zone 2 and Zone 3 regions. AIY is a unipolar neuron with both inputs, including those from AFD, in zone 2 and outputs to postsynaptic partners. We also quantified a reference region outside of AIY. Consistent with previous reports (Clark et al., 2006), we observed clear and qualitatively similar responses to thermal stimuli in the synaptic Zone 2 and Zone 3 regions. Although calcium responses were sometimes observed in the AIY soma, we could not correlate these soma responses to the thermal stimuli.

Electrophysiology—All electrophysiological experiments were performed with young adult hermaphrodites. An animal was immobilized on a glass coverslip by applying Vetbond Tissue Adhesive (3M Company, St Paul, MN) restricted to the dorsal head region. A short longitudinal incision was made along the glued region. The cuticle flap was folded back and glued to the coverslip, exposing AIYs neurons. The dissected worm preparation was treated with collagenase A (Roche Applied Science, catalogue number 10103578001, 0.5 mg/ml) for 10–15 s and perfused with the extracellular solution. Borosilicate glass pipettes were used as recording electrodes with a tip resistance ~ 20 MΩ. AIYs neurons were identified based on mCherry fluorescence driven by the *ttx-3* promoter. PSCs were recorded at a holding voltage of −60 mV under classical whole-cell configuration with a Multiclamp 700B amplifier (Molecular Devices, Sunnyvale, CA, USA) and analyzed with the Clampex software (version 10, Molecular Devices). Data were filtered at 2 kHz and sampled at 10 kHz. The extracellular solution contained (in mM) 140 NaCl, 5 KCl, 5 $CaCl_2$, 5 $MgCl_2$, 11 dextrose and 5 HEPES (pH 7.2). The pipette solution contained (in mM) 120 KCl, 20 KOH, 5 Tris, 0.25 $CaCl_2$, 4 $MgCl_2$, 36 sucrose, 5 EGTA, and 4 Na_2ATP (pH 7.2). Thermal ramps were achieved by superfusing the animals with extracellular solution that was warmed or cooled with a thermoelectric heater/cooler (SC-20/CL-100, Warner Instruments) similar to methods previously described (Ramot et al., 2008a). Temperature changes were measured close the worm head using the bead thermistor (TS-70B, Warner Instruments). Thermistor values were recorded in Clampex software simultaneously with electrophysiological data. Data analysis was performed in Clampfit (Molecular Devices) and Matlab (Mathworks). To account for sample-to-sample variation in AIY basal sPSC rate, a normalized warming-evoked sPSC rate was calculated by subtracting the sPSC rate during cooling from the sPSC rate during warming and presented in Figure 4F.

Modeling of AFD adaptation—After training, AFD response threshold adapts to a new temperature with time following an exponential function ($T_S=C*e^{-t/tau}$, Figure 1J). The change in T_S, ΔT_S, with an increment of time, Δt, at time t can be expressed as $\Delta T_S/\Delta t(t)=(-C(t)/tau)* e^{-t/tau}$. The value of C at time t, C(t), is the offset between current temperature, $T_H(t)$, and AFD threshold, $T_S(t)$, such that $C(t)=T_S(t)-T_H(t)$). Based on these three equations and the empirically calculated time constants for tau (derived from data in

Figure 1J), the AFD threshold can be calculated iteratively for a migrating animal by incrementing the T_S value with the derivative of T_S under present conditions, $T_S(t)=T_S(t-1)+\Delta T_S/\Delta t\ (t)^* \Delta t$, resulting in the model presented in (Figure S2X). Because tau is distinct for adaptation to higher and lower temperature, the appropriate tau was selected at each iteration depending on the relationship between T_S and T_H.

QUANTIFICATION AND STATISTICAL ANALYSIS

For calcium imaging experiments, quantification was performed in Matlab (MathWorks). For electrophysiology experiments, quantification was performed in ClampFit. For all experiments, statistical tests were performed in Matlab (MathWorks). Continuous data analyzed for statistical significance by non-parametric Kruskall-Wallis ANOVA followed by *post-hoc* comparisons with a two-tailed Wilcoxon rank sum test. Categorical data were analyzed for statistical significance by chi-squared analysis followed by pair-wise two-tailed Fisher's exact tests.

KEY RESOURCES TABLE

REAGENT or RESOURCE	SOURCE	IDENTIFIER
Antibodies		
Bacterial and Virus Strains		
Biological Samples		
Chemicals, Peptides, and Recombinant Proteins		
Critical Commercial Assays		
Deposited Data		
Experimental Models: Cell Lines		
Experimental Models: Organisms/Strains		
C. elegans: Strain GN71: *pkc-1(pg5) V*	Luo et al. 2014	N/A
C. elegans: Strain IK105: *pkc-1(nj1) V*	Caenorhabditis Genetics Center	WB strain: IK105 WormBase: WBvar00091271
C. elegans: Strain DCR3558 *olaIs23 [Pgcy-8::caPKC-1; Pgcy-8::tagRFP; Punc-122::dsRed]*	This paper	N/A
C. elegans: Strain DCR3055 *wyIs629 [Pgcy-8::GCaMP6s; Pgcy-8::mCherry; Punc-122::GFP]*	This paper	N/A
C. elegans: Strain DCR3245 *pkc-1(pg5); wyIs629 [Pgcy-8::GCaMP6s; Pgcy-8::mCherry; Punc-122::GFP]*	This paper	N/A
C. elegans: Strain DCR5099 *olaIs23 [Pgcy-8::caPKC-1; Pgcy-8::tagRFP; Punc-122::dsRed]; wyIs629 [Pgcy-8::GCaMP6s; Pgcy-8::mCherry; Punc-122::GFP]*	This paper	N/A
C. elegans: Strain DCR3056 *olaIs17 [Pmod-1::GCaMP6s; Pttx-3::mCherry; Punc-122::dsRed]*	This paper	N/A
C. elegans: Strain DCR3203 *pkc-1(pg5); olaIs17 [Pmod-1::GCaMP6s; Pttx-3::mCherry; Punc-122::dsRed],*	This paper	N/A
C. elegans: Strain DCR3572 *olaIs23 [Pgcy-8::caPKC-1; Pgcy-8::tagRFP; Punc-122::dsRed]; olaIs17 [Pmod-1::GCaMP6s; Pttx-3::mCherry; Punc-122::dsRed]*	This paper	N/A
C. elegans: Strain DCR3576 *oyIs85 [Pceh-36::caspase-3(p12)::nz; Pceh-36::cz::caspase-3(p17);*	This paper	N/A

REAGENT or RESOURCE	SOURCE	IDENTIFIER
Pstrx-1::GFP; Punc-122::dsRed]; olaIs17 [Pmod-1::GCaMP6s; Pttx-3::mCherry; Punc-122::dsRed]		
C. elegans: Strain DCR3670 *olaIs17 [Pmod-1::GCaMP6s; Pttx-3::mCherry; Punc-122::dsRed]; olaIs23 [Pgcy-8::caPKC-1; Pgcy-8::tagRFP; Punc-122::dsRed]; olaEx2125 [Pgcy-8::caspase-3(p12)::nz; Pgcy-8::cz::caspase-3(p17); Pgcy-8::tagRFP; Pmyo-3::mCherry]*	This paper	N/A
C. elegans: Strain DCR5586 *olaIs70 [Pgcy-8::CX36::mCherry; Pelt-7::GFP::NLS]*	This paper	N/A
C. elegans: Strain DCR5639 *olaIs72 [Pttx-3::sl2::CX36::mCherry; Pelt-7::mCherry::NLS]*	This paper	N/A
C. elegans: Strain DCR5793 *olaIs17 [Pmod-1::GCaMP6s; Pttx-3::mCherry; Punc-122::dsRed]; olaIs70 [Pgcy-8::CX36::mCherry; Pelt-7::GFP::NLS]; olaIs72 [Pttx-3::sl2::CX36::mCherry; Pelt-7::mCherry::NLS]*	This paper	N/A
C. elegans: Strain DCR5792 *wyIs629 [Pgcy-8::GCaMP6s; Pgcy-8::mCherry; Punc-122::GFP]; olaIs70 [Pgcy-8::CX36::mCherry; Pelt-7::GFP::NLS]; olaIs72 [Pttx-3::sl2::CX36::mCherry; Pelt-7::mCherry::NLS]*	This paper	N/A
C. elegans: Strain DCR5789 *olaIs17 [Pmod-1::GCaMP6s; Pttx-3::mCherry; Punc-122::dsRed]; olaIs70 [Pgcy-8::CX36::mCherry; Pelt-7::GFP::NLS]*	This paper	N/A
C. elegans: Strain DCR5790 *olaIs17 [Pmod-1::GCaMP6s; Pttx-3::mCherry; Punc-122::dsRed]; olaIs72 [Pttx-3::sl2::CX36::mCherry; Pelt-7::mCherry::NLS]*	This paper	N/A
C. elegans: Strain DCR5404 *olaIs17 [Pmod-1::GCaMP6s; Pttx-3::mCherry; Punc-122::dsRed]; olaIs23 [Pgcy-8::caPKC-1; Pgcy-8::tagRFP; Punc-122::dsRed]; olaEx3219 [Pgcy-8::CX36::mCherry; Pttx-3::sl2::CX36::mCherry; Pmyo-3::mCherry]*	This paper	N/A
C. elegans: Strain DCR5380 *olaIs17 [Pmod-1::GCaMP6s; Pttx-3::mCherry; Punc-122::dsRed]; olaEx3219 [Pgcy-8::CX36::mCherry; Pttx-3::sl2::CX36::mCherry; Pmyo-3::mCherry]*	This paper	N/A
Oligonucleotides		
Genotyping primer: pkc1-nj1-f: att cca aaa tct gcc aaa cg	This paper	N/A
Genotyping primer: pkc1-nj1-r: cta aaa acc gac acc ctt gg	This paper	N/A
Genotyping primer: pkc1-pg5_F2: agctggcacaacttggactt	This paper	N/A
Genotyping primer: pkc1-pg5_R2: cgaatgctgaaaaacccaaa	This paper	N/A
Cloning primer F57F5.5b Forward: GGGGACAAGTTTGTACAAAAAAGCAGGCTAA ATGAGTTTTGATTGTTTGGTATACGATG	This paper	N/A
Cloning primer F57F5.5b Reverse: GGGGACCACTTTGTACAAGAAAGCTGGGTC GTAGGTAAAATGCGGATTGATAAATG	This paper	N/A
Recombinant DNA		
Plasmid: DACR1040 Pgcy-8::GCaMP6s	This paper	N/A
Plasmid: DACR1193 Pgcy-8::caspase-3(p12)::nz	Luo et al. 2014	N/A
Plasmid: DACR1194 Pgcy-8::caspase-3(p17)	Luo et al. 2014	N/A
Plasmid: DACR1286 Pmod-1::GCaMP6s	This paper	N/A
Plasmid: DACR2397 Pttx-3::sl2::CX36::mCherry	This paper	N/A
Plasmid: DACR2398 Pgcy-8::CX36::mCherry	This paper	N/A

REAGENT or RESOURCE	SOURCE	IDENTIFIER
Plasmid: DACR2549 Pgcy-8::caPKC-1	This paper	N/A
Software and Algorithms		
MagatAnalyzer	Gershow et al. 2012	
LabView 2011	National Instruments	
Metamorph	Molecular Devices	
ClampEx 10	Molecular Devices	
ClampFit 10.7	Molecular Devices	
Matlab R2016a	MathWorks	
Other		

Supplementary Material

Refer to Web version on PubMed Central for supplementary material.

Acknowledgments

We thank members of the Colón-Ramos lab and the Samuel lab for their thoughtful comments on the project. We also thank Miriam Goodman (Stanford University), Damon Clark (Yale University) and Piali Sengupta (Brandeis University) for thoughtful comments on the project and the manuscript. We thank the *Caenorhabditis* Genetics Center (supported by the National Institutes of Health (NIH), Office of Research Infrastructure Programs; P40 OD010440) for strains, and the Bargmann lab (Rockefeller University), the Goodman lab (Stanford University), the Schafer lab (Medical Research Council) and the Looger lab (Janelia Research Campus) for reagents. We thank Z. Altun (www.wormatlas.org) for diagrams used in figures. We thank the Research Center for Minority Institutions program and the Instituto de Neurobiología de la Universidad de Puerto Rico for providing a meeting and brainstorming platform. We thank the students of the Neural Systems and Behavior course from Marine Biological Laboratories at Woods Hole, particularly Ranran "Annette" Li, Raina Rhoades, Ernesto Cabezas and Ifedayo-Emmanuel Adeyefa-Olasupo. This work was partially conducted at the Marine Biological Laboratories at Woods Hole, under a Whitman research award to D.A.C.-R. Support for J.D.H. was provided by the Ruth L. Kirschstein NRSA (NIH-NIMH-F32MH105063). Research was supported by the National Science Foundation (NSF IOS 1353845 to D.A.C.-R, and PHY-0957185 to A.D.T.S) and the National Institutes of Health (8DP1GM105383 and 1P01GM103770 to A.D.T.S, and R01MH085927 to Z.-W.W).

References

Aoki I, Mori I. Molecular biology of thermosensory transduction in C. elegans. Curr Opin Neurobiol. 2015; 34:117–124. [PubMed: 25840145]

Basu J, Siegelbaum SA. The Corticohippocampal Circuit, Synaptic Plasticity, and Memory. Cold Spring Harb Perspect Biol. 2015; 7

Beverly M, Anbil S, Sengupta P. Degeneracy and neuromodulation among thermosensory neurons contribute to robust thermosensory behaviors in Caenorhabditis elegans. J Neurosci. 2011; 31:11718–11727. [PubMed: 21832201]

Biron D, Shibuya M, Gabel C, Wasserman SM, Clark DA, Brown A, Sengupta P, Samuel AD. A diacylglycerol kinase modulates long-term thermotactic behavioral plasticity in C. elegans. Nat Neurosci. 2006; 9:1499–1505. [PubMed: 17086178]

Biron D, Wasserman S, Thomas JH, Samuel AD, Sengupta P. An olfactory neuron responds stochastically to temperature and modulates Caenorhabditis elegans thermotactic behavior. Proc Natl Acad Sci U S A. 2008; 105:11002–11007. [PubMed: 18667708]

Brenner S. The genetics of Caenorhabditis elegans. Genetics. 1974; 77:71–94. [PubMed: 4366476]

Broussard GJ, Liang R, Tian L. Monitoring activity in neural circuits with genetically encoded indicators. Front Mol Neurosci. 2014; 7:97. [PubMed: 25538558]

Chao YC, Chen CC, Lin YC, Breer H, Fleischer J, Yang RB. Receptor guanylyl cyclase-G is a novel thermosensory protein activated by cool temperatures. EMBO J. 2015; 34:294–306. [PubMed: 25452496]

Chelur DS, Chalfie M. Targeted cell killing by reconstituted caspases. Proc Natl Acad Sci U S A. 2007; 104:2283–2288. [PubMed: 17283333]

Chen TW, Wardill TJ, Sun Y, Pulver SR, Renninger SL, Baohan A, Schreiter ER, Kerr RA, Orger MB, Jayaraman V, et al. Ultrasensitive fluorescent proteins for imaging neuronal activity. Nature. 2013; 499:295–300. [PubMed: 23868258]

Chi CA, Clark DA, Lee S, Biron D, Luo L, Gabel CV, Brown J, Sengupta P, Samuel AD. Temperature and food mediate long-term thermotactic behavioral plasticity by association-independent mechanisms in C. elegans. J Exp Biol. 2007; 210:4043–4052. [PubMed: 17981872]

Cho CE, Brueggemann C, L'Etoile ND, Bargmann CI. Parallel encoding of sensory history and behavioral preference during Caenorhabditis elegans olfactory learning. Elife. 2016; 5

Clark DA, Biron D, Sengupta P, Samuel AD. The AFD sensory neurons encode multiple functions underlying thermotactic behavior in Caenorhabditis elegans. J Neurosci. 2006; 26:7444–7451. [PubMed: 16837592]

Colon-Ramos DA, Margeta MA, Shen K. Glia promote local synaptogenesis through UNC-6 (netrin) signaling in C. elegans. Science. 2007; 318:103–106. [PubMed: 17916735]

Colosimo ME, Brown A, Mukhopadhyay S, Gabel C, Lanjuin AE, Samuel AD, Sengupta P. Identification of thermosensory and olfactory neuron-specific genes via expression profiling of single neuron types. Curr Biol. 2004; 14:2245–2251. [PubMed: 15620651]

Davis RL. Traces of Drosophila memory. Neuron. 2011; 70:8–19. [PubMed: 21482352]

Epstein ML, Gilula NB. A study of communication specificity between cells in culture. J Cell Biol. 1977; 75:769–787. [PubMed: 562887]

Fain GL, Matthews HR, Cornwall MC, Koutalos Y. Adaptation in vertebrate photoreceptors. Physiol Rev. 2001; 81:117–151. [PubMed: 11152756]

Fesenko EE, Kolesnikov SS, Lyubarsky AL. Induction by cyclic GMP of cationic conductance in plasma membrane of retinal rod outer segment. Nature. 1985; 313:310–313. [PubMed: 2578616]

Garrity PA, Goodman MB, Samuel AD, Sengupta P. Running hot and cold: behavioral strategies, neural circuits, and the molecular machinery for thermotaxis in C. elegans and Drosophila. Genes Dev. 2010; 24:2365–2382. [PubMed: 21041406]

Gershow M, Berck M, Mathew D, Luo L, Kane EA, Carlson JR, Samuel AD. Controlling airborne cues to study small animal navigation. Nat Methods. 2012; 9:290–296. [PubMed: 22245808]

Gjorgjieva J, Drion G, Marder E. Computational implications of biophysical diversity and multiple timescales in neurons and synapses for circuit performance. Curr Opin Neurobiol. 2016; 37:44–52. [PubMed: 26774694]

Gray JM, Hill JJ, Bargmann CI. A circuit for navigation in Caenorhabditis elegans. Proc Natl Acad Sci U S A. 2005; 102:3184–3191. [PubMed: 15689400]

Hedgecock EM, Russell RL. Normal and mutant thermotaxis in the nematode Caenorhabditis elegans. Proc Natl Acad Sci U S A. 1975; 72:4061–4065. [PubMed: 1060088]

Hobert O, Mori I, Yamashita Y, Honda H, Ohshima Y, Liu Y, Ruvkun G. Regulation of interneuron function in the C. elegans thermoregulatory pathway by the ttx-3 LIM homeobox gene. Neuron. 1997; 19:345–357. [PubMed: 9292724]

Inada H, Ito H, Satterlee J, Sengupta P, Matsumoto K, Mori I. Identification of guanylyl cyclases that function in thermosensory neurons of Caenorhabditis elegans. Genetics. 2006; 172:2239–2252. [PubMed: 16415369]

Ito H, Inada H, Mori I. Quantitative analysis of thermotaxis in the nematode Caenorhabditis elegans. J Neurosci Methods. 2006; 154:45–52. [PubMed: 16417923]

Kimura KD, Miyawaki A, Matsumoto K, Mori I. The C. elegans thermosensory neuron AFD responds to warming. Curr Biol. 2004; 14:1291–1295. [PubMed: 15268861]

Ko KI, Root CM, Lindsay SA, Zaninovich OA, Shepherd AK, Wasserman SA, Kim SM, Wang JW. Starvation promotes concerted modulation of appetitive olfactory behavior via parallel neuromodulatory circuits. Elife. 2015; 4

Kocabas A, Shen CH, Guo ZV, Ramanathan S. Controlling interneuron activity in Caenorhabditis elegans to evoke chemotactic behaviour. Nature. 2012; 490:273–277. [PubMed: 23000898]

Komatsu H, Mori I, Rhee JS, Akaike N, Ohshima Y. Mutations in a cyclic nucleotide-gated channel lead to abnormal thermosensation and chemosensation in C. elegans. Neuron. 1996; 17:707–718. [PubMed: 8893027]

Kuhara A, Ohnishi N, Shimowada T, Mori I. Neural coding in a single sensory neuron controlling opposite seeking behaviours in Caenorhabditis elegans. Nat Commun. 2011; 2:355. [PubMed: 21673676]

Kuhara A, Okumura M, Kimata T, Tanizawa Y, Takano R, Kimura KD, Inada H, Matsumoto K, Mori I. Temperature sensing by an olfactory neuron in a circuit controlling behavior of C. elegans. Science. 2008; 320:803–807. [PubMed: 18403676]

Li Z, Liu J, Zheng M, Xu XZ. Encoding of both analog- and digital-like behavioral outputs by one C. elegans interneuron. Cell. 2014; 159:751–765. [PubMed: 25417153]

Luo L, Clark DA, Biron D, Mahadevan L, Samuel AD. Sensorimotor control during isothermal tracking in Caenorhabditis elegans. J Exp Biol. 2006; 209:4652–4662. [PubMed: 17114399]

Luo L, Cook N, Venkatachalam V, Martinez-Velazquez LA, Zhang X, Calvo AC, Hawk J, MacInnis BL, Frank M, Ng JH, et al. Bidirectional thermotaxis in Caenorhabditis elegans is mediated by distinct sensorimotor strategies driven by the AFD thermosensory neurons. Proc Natl Acad Sci U S A. 2014; 111:2776–2781. [PubMed: 24550307]

Mayford M, Siegelbaum SA, Kandel ER. Synapses and memory storage. Cold Spring Harb Perspect Biol. 2012; 4

Mello C, Fire A. DNA transformation. Methods Cell Biol. 1995; 48:451–482. [PubMed: 8531738]

Merritt C, Seydoux G. Transgenic solutions for the germline. WormBook. 2010:1–21.

Miyawaki A, Griesbeck O, Heim R, Tsien RY. Dynamic and quantitative Ca2+ measurements using improved cameleons. Proc Natl Acad Sci U S A. 1999; 96:2135–2140. [PubMed: 10051607]

Mohri A, Kodama E, Kimura KD, Koike M, Mizuno T, Mori I. Genetic control of temperature preference in the nematode Caenorhabditis elegans. Genetics. 2005; 169:1437–1450. [PubMed: 15654086]

Mori I, Ohshima Y. Neural regulation of thermotaxis in Caenorhabditis elegans. Nature. 1995; 376:344–348. [PubMed: 7630402]

Narayan A, Laurent G, Sternberg PW. Transfer characteristics of a thermosensory synapse in Caenorhabditis elegans. Proc Natl Acad Sci U S A. 2011; 108:9667–9672. [PubMed: 21606366]

Ohnishi N, Kuhara A, Nakamura F, Okochi Y, Mori I. Bidirectional regulation of thermotaxis by glutamate transmissions in Caenorhabditis elegans. EMBO J. 2011; 30:1376–1388. [PubMed: 21304490]

Okochi Y, Kimura KD, Ohta A, Mori I. Diverse regulation of sensory signaling by C. elegans nPKC-epsilon/eta TTX-4. EMBO J. 2005; 24:2127–2137. [PubMed: 15920475]

Rabinowitch I, Chatzigeorgiou M, Zhao B, Treinin M, Schafer WR. Rewiring neural circuits by the insertion of ectopic electrical synapses in transgenic C. elegans. Nat Commun. 2014; 5:4442. [PubMed: 25026983]

Ramot D, MacInnis BL, Goodman MB. Bidirectional temperature-sensing by a single thermosensory neuron in C. elegans. Nat Neurosci. 2008a; 11:908–915. [PubMed: 18660808]

Ramot D, MacInnis BL, Lee HC, Goodman MB. Thermotaxis is a robust mechanism for thermoregulation in Caenorhabditis elegans nematodes. J Neurosci. 2008b; 28:12546–12557. [PubMed: 19020047]

Root CM, Ko KI, Jafari A, Wang JW. Presynaptic facilitation by neuropeptide signaling mediates odor-driven food search. Cell. 2011; 145:133–144. [PubMed: 21458672]

Ryu WS, Samuel AD. Thermotaxis in Caenorhabditis elegans analyzed by measuring responses to defined Thermal stimuli. J Neurosci. 2002; 22:5727–5733. [PubMed: 12097525]

Sieburth D, Madison JM, Kaplan JM. PKC-1 regulates secretion of neuropeptides. Nat Neurosci. 2007; 10:49–57. [PubMed: 17128266]

Son H, Madelian V, Carpenter DO. The translocation and involvement of protein kinase C in mossy fiber-CA3 long-term potentiation in hippocampus of the rat brain. Brain Res. 1996; 739:282–292. [PubMed: 8955949]

Stiernagle T. Maintenance of C. elegans. WormBook. 2006:1–11.

Takeishi A, Yu YV, Hapiak VM, Bell HW, O'Leary T, Sengupta P. Receptor-type Guanylyl Cyclases Confer Thermosensory Responses in C. elegans. Neuron. 2016; 90:235–244. [PubMed: 27041501]

Tian L, Hires SA, Looger LL. Imaging neuronal activity with genetically encoded calcium indicators. Cold Spring Harb Protoc. 2012; 2012:647–656. [PubMed: 22661439]

Tsukada Y, Yamao M, Naoki H, Shimowada T, Ohnishi N, Kuhara A, Ishii S, Mori I. Reconstruction of Spatial Thermal Gradient Encoded in Thermosensory Neuron AFD in Caenorhabditis elegans. J Neurosci. 2016; 36:2571–2581. [PubMed: 26936999]

Ventimiglia D, Bargmann CI. Diverse modes of synaptic signaling, regulation, and plasticity distinguish two classes of C. elegans glutamatergic neurons. Elife. 2017; 6

Wang D, O'Halloran D, Goodman MB. GCY-8, PDE-2, and NCS-1 are critical elements of the cGMP-dependent thermotransduction cascade in the AFD neurons responsible for C. elegans thermotaxis. J Gen Physiol. 2013; 142:437–449. [PubMed: 24081984]

White JG, Southgate E, Thomson JN, Brenner S. The structure of the nervous system of the nematode Caenorhabditis elegans. Philos Trans R Soc Lond B Biol Sci. 1986; 314:1–340. [PubMed: 22462104]

Yau KW, Nakatani K. Light-suppressible, cyclic GMP-sensitive conductance in the plasma membrane of a truncated rod outer segment. Nature. 1985; 317:252–255. [PubMed: 2995816]

Yu YV, Bell HW, Glauser DA, Van Hooser SD, Goodman MB, Sengupta P. CaMKI-dependent regulation of sensory gene expression mediates experience-dependent plasticity in the operating range of a thermosensory neuron. Neuron. 2014; 84:919–926. [PubMed: 25467978]

Zisopoulou S, Asimaki O, Leondaritis G, Vasilaki A, Sakellaridis N, Pitsikas N, Mangoura D. PKC-epsilon activation is required for recognition memory in the rat. Behav Brain Res. 2013; 253:280–289. [PubMed: 23911427]

Highlights

- Sensory adaptation and presynaptic plasticity act within a single neuron *in vivo*
- Integration of these plasticity mechanisms underpins a temperature preference memory
- Sensory adaptation enables migrating animal to detect temperature changes
- Presynaptic plasticity transforms this thermosensory information into a preference

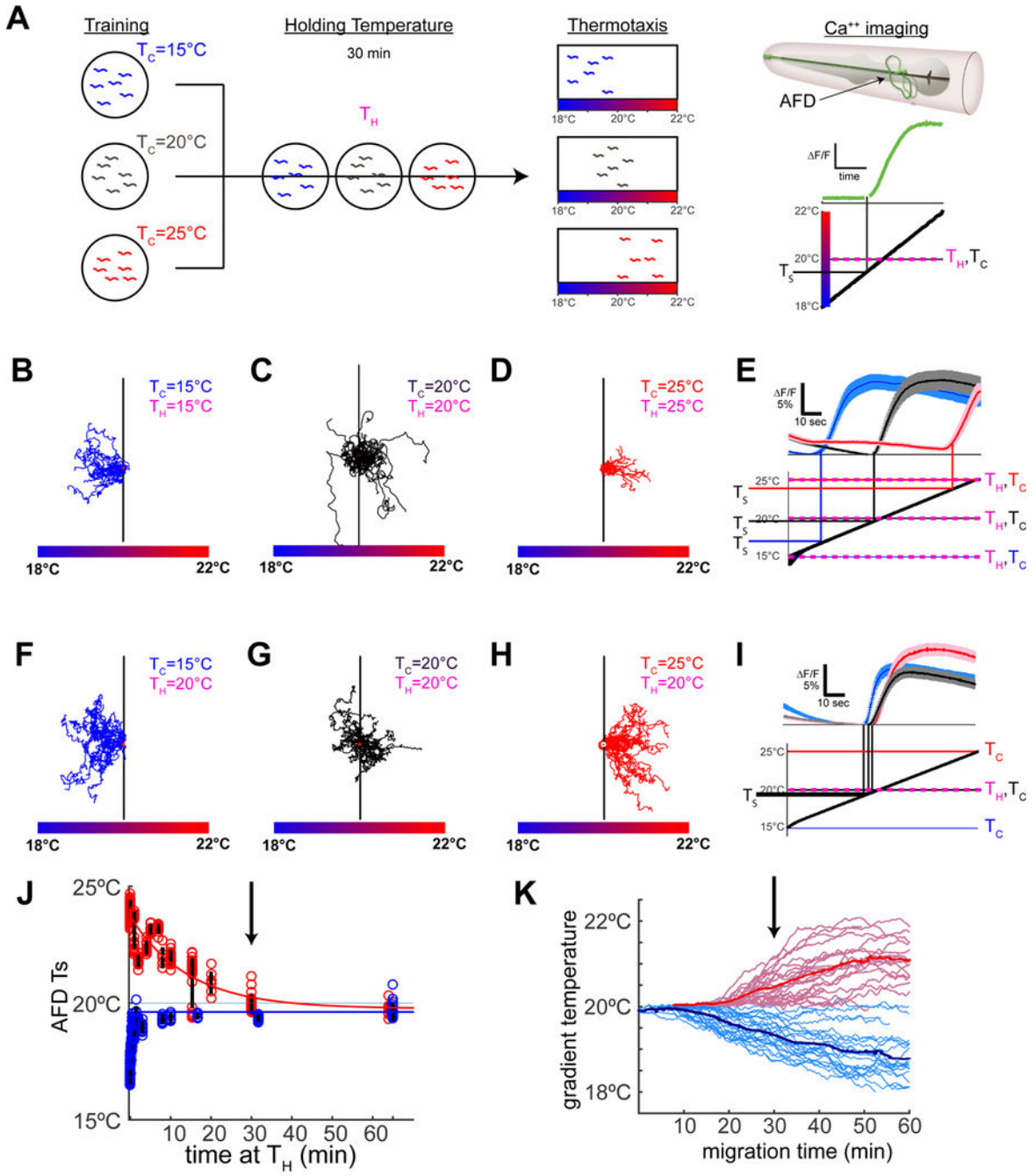

Figure 1. AFD thermosensory threshold adapts within minutes and does not represent the temperature preference memory

(**A**) Schematic illustration of the experimental paradigms. Animals cultivated for 4hr either at 15°C, 20°C or 25°C ("Training") were then held at specified temperatures ("Holding Temperature", T_H) for 30 minutes prior to being tested in behavioral assays ("Thermotaxis") or calcium imaging in specific neurons ("Ca^{++} imaging"). The response of a single AFD neuron (green trace) is illustrated as a change in fluorescence (ΔF/F) over time when applying a linear thermal ramp (thick black diagonal line) from 18°C to 22°C. (**B–E**) Worms trained at 15°C, 20°C, or 25°C were examine d for thermotaxis behavior in **B–D** and

calcium imaging in AFD in **E**. The mean AFD response threshold for T_C=15°C was 16.9°C +/− 0.5°C (blue trace), T_C=20°C was 19.9°C +/− 0.5°C (black trace), and T_C=25°C was 23.9°C +/− 0.4°C (red trace). Note that when T_H=T_C, AFD response threshold (T_S) correlates with the T_C, consistent with previous reports (Clark et al., 2006; Kimura et al., 2004; Ramot et al., 2008a). Traces for individual animals in Figure S1C–E. (**F–I**) As in **B–E**, but animals were held at T_H=20°C for 30 minutes prior to thermotaxis behavior in **F–H** or calcium imaging in **I**. Note that, regardless of T_H, animals retain the cultivation temperature memory and perform the thermotaxis behavior (**F–H** consistent with (Hedgecock and Russell, 1975)). In contrast, the AFD response threshold (T_S) adapts to the holding temperature (T_H) and all animals, regardless of cultivation temperature memory, respond near T_H=20°C as shown in **I** (T_S=19.4°C +/−0.1°C for T_C=15°C, 19.8°C +/−0.2°C for T_C=20°C, and 19.9°C +/−0.3°C for T_C=25°C). Traces for individual animals are in Figure S1F–H. (**J**) AFD adaption kinetics were assessed in a training paradigm as described in **A**, but with varying amounts of time held at T_H. The threshold T_S is plotted for each duration of holding at T_H. The time course of adaptation in AFD for cooling temperatures (T_H=20°C & T_C=25°C, tau=14min) is slower than that observed for warming temperatures (T_H=20°C & T_C=15°C, tau=45sec). Yet, note that by 30 minutes (black arrow) sensory threshold responses in AFD have adapted to very near T_H regardless of T_C. See also Figure S2. (**K**) Behavioral kinematics showing migration of animals over time illustrate that migration onset correlates well with AFD adaptation kinetics, with peak migration occurring around 30 minutes after worms were placed at 20°C (black vertical arrow). See also Figure S2X. Error bars denote SEM.

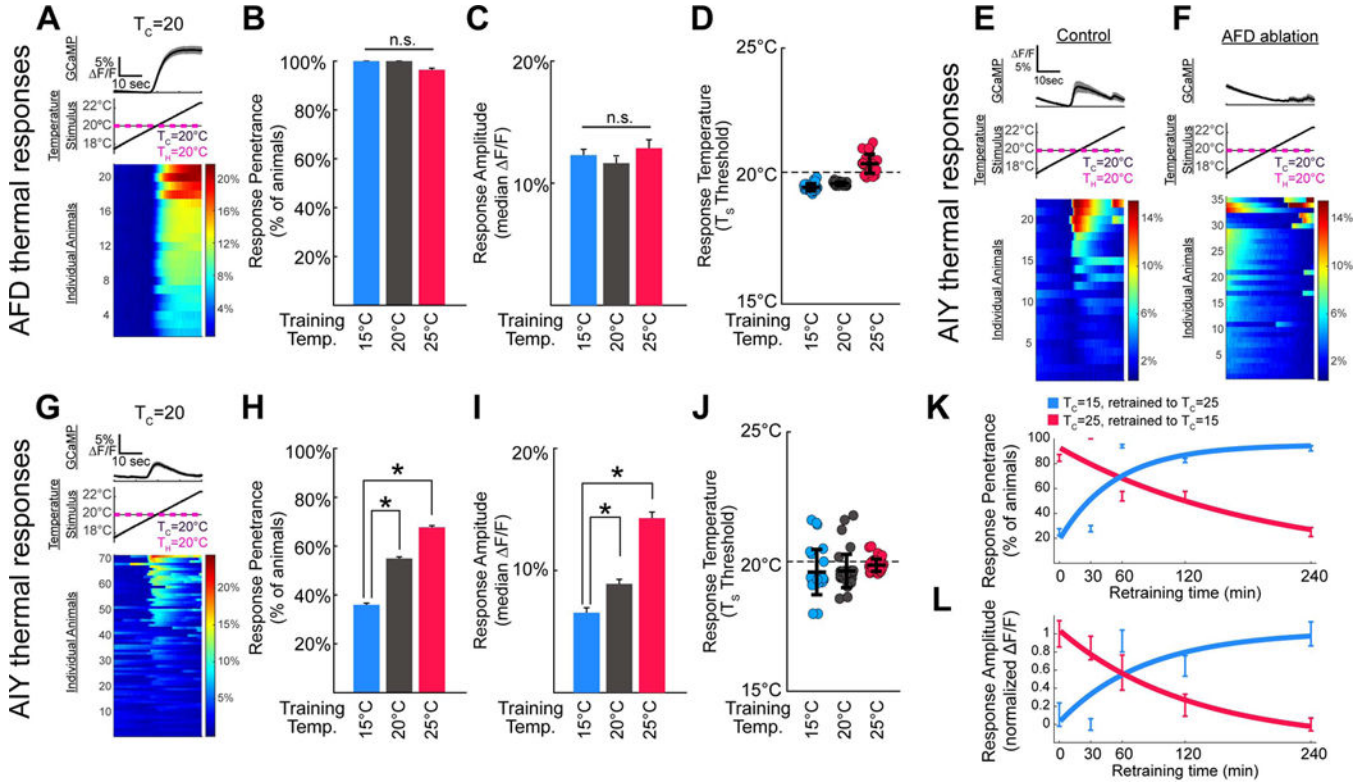

Figure 2. Postsynaptic response in AIY correlates with the cultivation temperature memory

(**A**) Illustration of the experimental paradigm, shown in AFD for a single condition (T_C=20°C; for heat maps of other conditions please see Figure S4). The average GCaMP signal is represented in the top panel, stimulus protocol in the middle panel and individual responses in the bottom panel, with each row representing a single worm. Total number of worms tested are represented to the left of the calcium traces (under "individual animals"), and percentage change ΔF/F is represented in the color bar to the right. (**B–D)** Comparison of calcium dynamics of AFD neurons of animals trained at T_C=15°C (blue), T_C=20°C (grey), or T_C =25°C (red) then tested at T_H=20°C. Under all training conditions, the AFD of nearly every animal tested had detectable responses to the warming stimulus, with no significant effect of training condition (n=28, 21, and 28 respectively), as shown in **B**. Response amplitudes were similar among groups with no significant effect of training condition, as shown in **C**. In each case, the threshold for AFD thermal response was near the testing temperature, T_H, rather than the training temperature T_C, as shown in **D.** (**E,F**) AIY imaging reveals an AFD-dependent thermally evoked response near the threshold for AFD consistent with previous studies (Clark et al., 2006). Calcium dynamics of single AIY neurons in wild-type in **E** or AFD-ablated in **F** animals; see also Figure S3. (**G–J**) Animals trained as in **A–D** at T_C=15°C (blue), T_C =20°C (grey), or T_C =25°C (red) then tested at T_H=20°C, but with calcium imaging performed in AIY (the AFD postsynaptic partner). Note that while AFD responds robustly in all conditions, as shown in **B** and **C**, the AIY response frequency in **H** and amplitude in **I** varies significantly depending on the cultivation temperature memory. Like AFD, responses are observed near the testing temperature, T_S (we note additional AFD-independent response were also seen, and account for the increase

variability in **J** as compared to **D** (see also Figure S3)). (**K–L**) AIY response properties change with kinetics that mirrors those of behavioral memory. After initial training at T_C=15°C (blue) or T_C=25°C (red), animals were retrained for varying amounts of time at 25°C or 15°C, respectively. Vertical bars represent SEM with n=12–13 animals per time point for initial T_C=25°C in red and n=13–24 animals per time point for initial T_C=15°C in blue. Solid think lines represent exponential fits for response penetrance in **K** (red R^2=0.79 and blue R^2=0.76) and response amplitude in **L** (red R^2=0.98 and blue R^2=0.67). We note that a sigmoidal curve fit, particularly for shifts from T_C=15°C (in blue), could also fit the data. But importantly, our findings indicate that the adaptability of response penetrance and amplitude in AIY follow a time-course similar to that seen for the timing of behavioral retraining. Consistent with **G–J**, both the AIY response penetrance in **K** and amplitude in **L** correlate with the initial behavioral preference. These features are also stable for 30min, and then gradually reverse after 1 hour with complete reversion seen by 4 hours of retraining. Our observations closely match previous reports of the time-course for retraining of the behavioral memory (Hedgecock and Russell, 1975). * denotes $p<0.05$ by Mann-Whitney-Wilcoxon test for continuous amplitude data and by Fisher's Exact test for penetrance data. Error bars denote SEM.

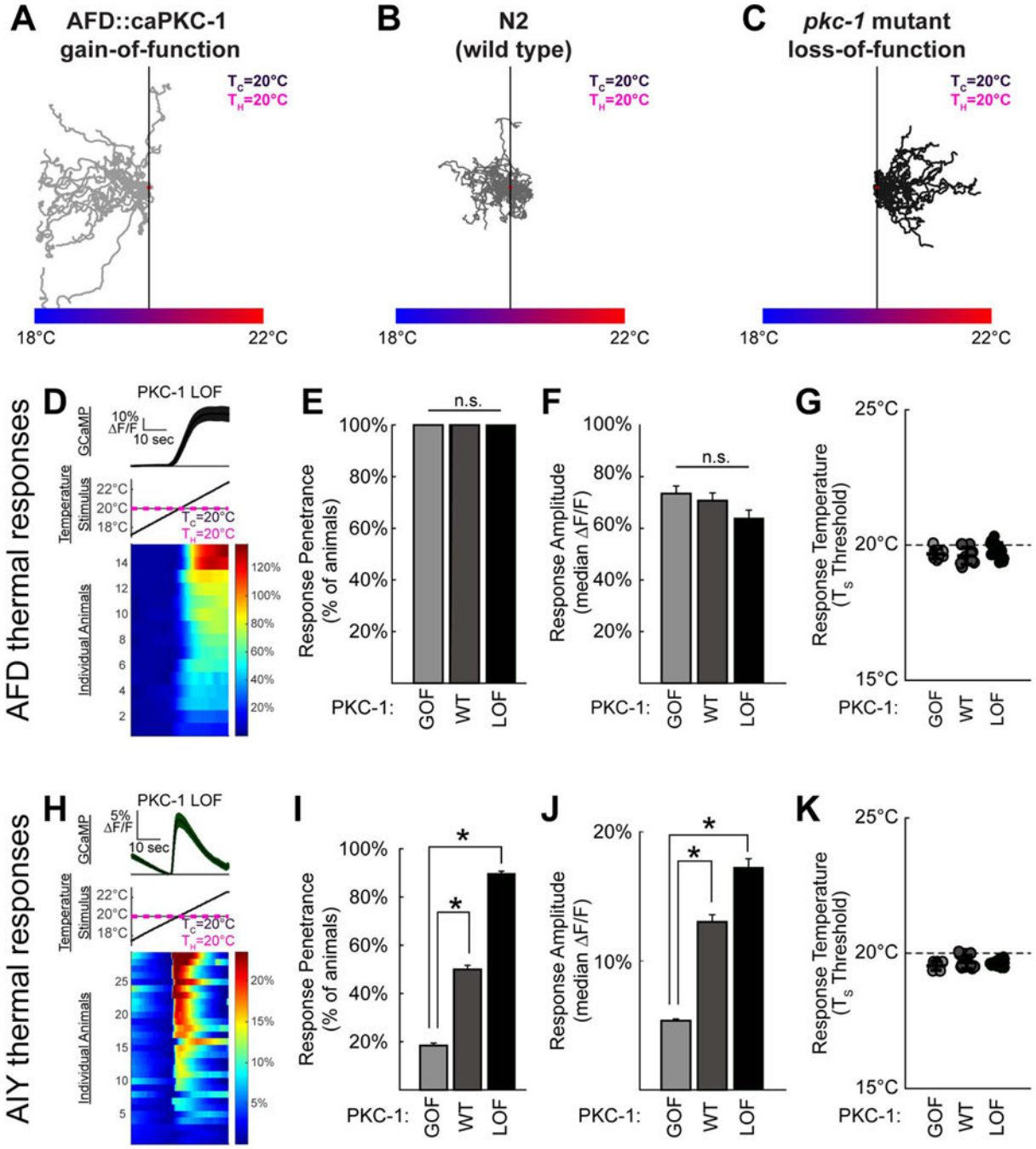

Figure 3. PKC-1 acts in AFD to control AIY response probability and T_C memory

(**A–C**) PKC-1 in AFD affects temperature preference regardless of previous experience. Expression of a constitutively active form of PKC-1 in the sensory neuron AFD (AFD::caPKC-1 GOF) produces worms that perform experience-independent negative thermotaxis, as shown in **A**, while worms with a loss-of-function mutation in PKC-1 (PKC-1 LOF) perform positive thermotaxis as shown in **C**, and regardless of T_C experience (Okochi et al., 2005). Wild-type worms trained at T_C=20°C show little bias when placed at the training temperature, as shown in **B**. (**D–G**) Comparison of calcium dynamics of AFD

neurons in animals expressing PKC-1 gain-of-function specifically in AFD (GOF, light gray), wild-type for PKC-1 (WT, gray), or PKC-1 loss of function mutants (LOF, black) each with $T_C = T_H = 20°C$. AFD response are shown for a single condition, PKC-1 LOF, in **D** to illustrate the experimental data (similar to Figure 2; for heat maps of other conditions please see Figure S4). For each of the PKC-1 conditions, every animal tested had detectable responses to the warming stimulus and amplitude, with no significant effect of genotype (n=10, 11, and 15 respectively), as shown in **E** and **F**. In each case, the threshold for AFD thermal response was near the testing temperature, T_H, as shown in **G**. (**H–K**) As in **D–G**, but in AIY (the AFD postsynaptic partner). Note that while responses in AFD are not affected by PKC-1 genetic manipulations (as shown in **E** and **F** and consistent with earlier observations (Luo et al., 2014)), AIY response frequency in **I** and amplitude in **J** varies depending on PKC-1 state within AFD. Also, note that these changes phenocopy AIY responses in animals trained to perform negative or positive thermotaxis, respectively (see Figure 2H–J and S4). * denotes $p<0.05$ by Mann-Whitney-Wilcoxon for continuous amplitude data and by Fisher's Exact test for penetrance data. Error bars denote SEM.

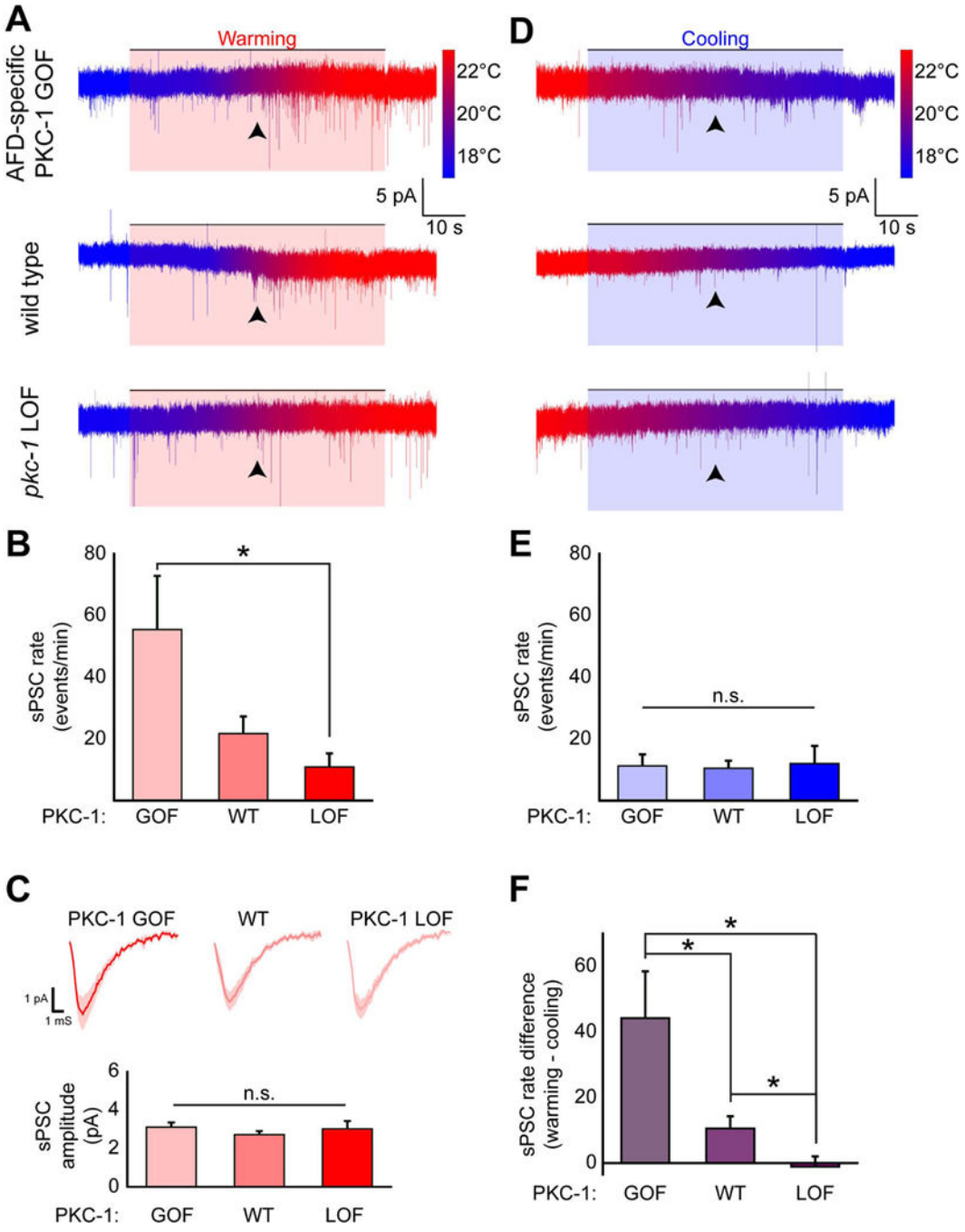

Figure 4. PKC-1 enhances warming evoked presynaptic output onto AIY

(**A**) Representative traces of AIY whole-cell currents recorded at a holding voltage of −60 mV from animals either expressing a gain-of-function constitutively active form of PKC-1 in AFD ("AFD-specific PKC-1 GOF" in top trace), endogenous wild-type *pkc-1*+ ("wild type" in middle trace), or a loss-of-function mutation in the *pkc-1* gene ("*pkc-1* LOF" in bottom trace). Animals in these recordings were cultivated at T_C=20°C, then subjected to a thermal ramp from approximately 16°C to 25°C with temperature indicated by the color of the trace (reference bar to right of trace, identical between samples, see also **Methods**). The upward

temperature shift, a stimulus which evokes calcium transients (e.g. see Fig S2) and depolarization (Ramot et al., 2008a) in AFD, is shaded in red and labeled as “Warming”. Arrowheads indicate 20°C in the temperature ramp. Please note burst of spontaneous post-synaptic currents (sPSC) following the arrowheads during warming ramps, but not cooling ramps (in **D**), and differences among genotypes. (**B**) Statistical comparisons of the rate of sPSCs in AIY during this warming stimulus in AFD-specific PKC-1 GOF animals, wild-type and *pkc-1* LOF mutant animals. (**C**) Averaged sPSCs from the different genotypes (top traces for indicated genotypes) and quantification of mean sPSC amplitude (bottom graph) between genotypes. (**D**) After the upward thermal ramp, animals were subjected to a downward thermal ramp, a stimulus that produces calcium decrement (e.g. see Fig S2) and hyperpolarization (Ramot et al., 2008a) in AFD, shaded in blue and labeled as “Cooling”. Genotype order as in (**A**) and arrowheads indicate 20°C in the temperature r amp. (**E**) Statistical comparisons of sPSC rate during downward thermal ramp. (**F**) Comparison of sPSC frequency differences (frequency during warming minus frequency during cooling) across the genotypes. Note that the normalized sPSC rate (see **Methods**) reveals a significant difference between the three genotypes. * denotes $p<0.05$ by Mann-Whitney-Wilcoxon test. Error bars denote SEM.

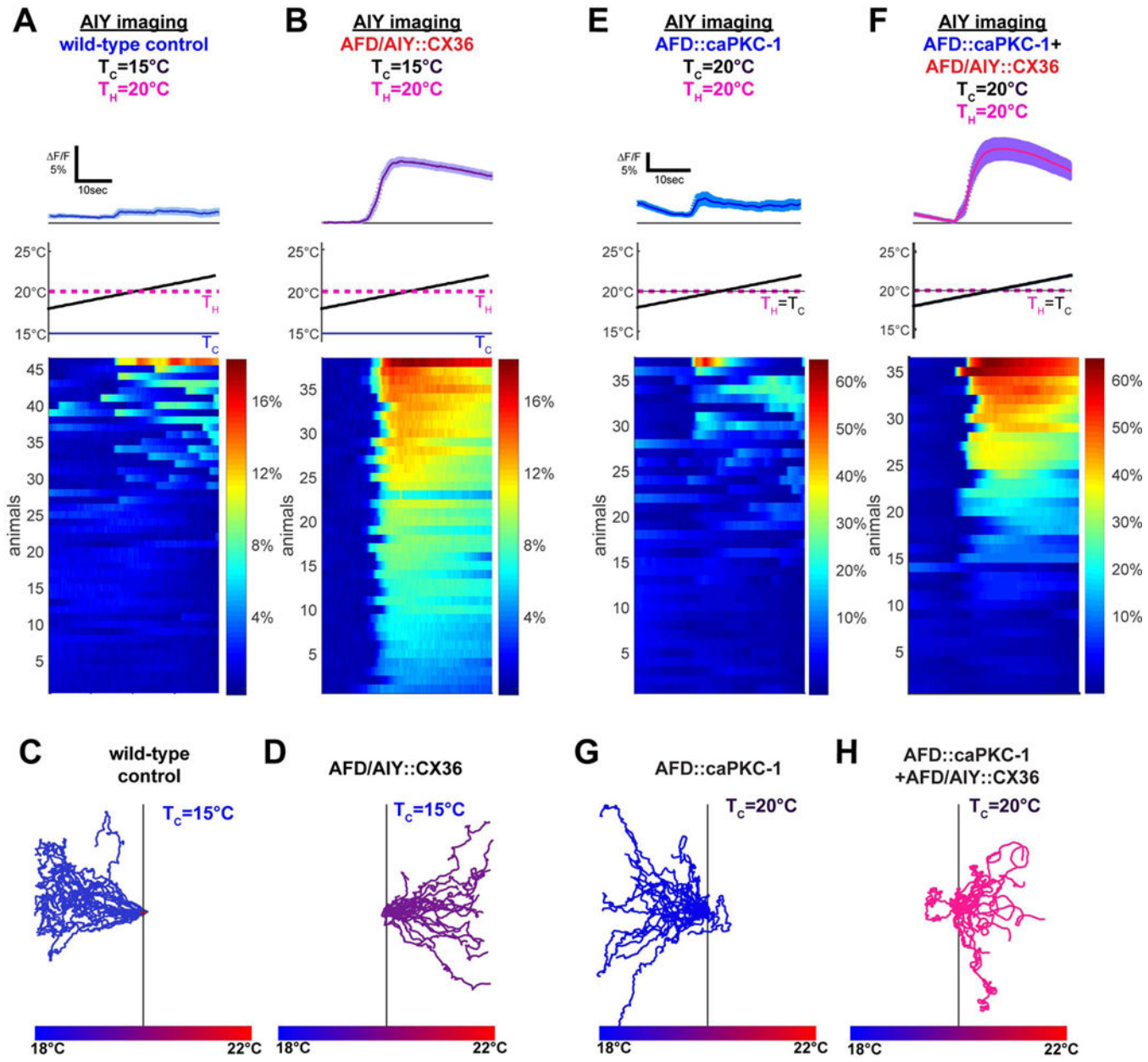

Figure 5. AFD to AIY connectivity actuates the thermal preference behavior

(**A**) Wild-type animals tested after adaptation above cultivation temperature (T_C=15°C<T_H=20°C) have weak and infrequent AIY responses near T_H (9/46 response penetrance, T_S=19.0°C +/−0.7°C). (**B**) Under the same training conditions, ectopic expression of the gap junction protein CX36 in AFD and AIY (AFD/AIY::CX36) produces responses in AIY that mirror AFD responses (38/38 response penetrance, T_S=19.0°C +/−0.2°C), suggesting this manipulation creates a strong positive coupling between AFD and AIY (see response kinetic analysis and quantification in Figure S5) (**C**) Worms cultivated at T_C=15°C perform negative thermotaxis on a thermal gradient centered at 20°C. (**D**) Expression of the gap junction protein CX36 in both AFD and AIY produces worms that perform positive thermotaxis under the same conditions. (**E**) Expression of a constitutively

active form of PKC-1 in AFD reduces AIY response frequency when T_C=T_H=20°C (13/37 response penetrance, T S=19.2°C +/−0.5°C). (**F**) AFD/AIY::CX36 increases AIY response frequency even in the presence of the AFD::caPKC-1 transgene (24/36 response penetrance, T_S=19.3°C +/−0.2°C). Because of genetic linkage between the AFD::caPKC-1 transgene and the AFD::CX36 transgene, experiments in **F** (and **H**) were performed with unstable extrachromosomal lines as described in the **Methods** (unlike experiments in **B** and **D**, which were performed with an integrated CX36 transgenes). (**G–H**) In contrast to worms expressing constitutively active PKC-1 in AFD, which perform negative thermotaxis when T_C=20°C as shown in **G**, expression of CX36 in AFD and AIY suppresses the phenotype of AFD::caPKC-1 animals and results in positive thermotaxis as shown in **H**. For all experiments with CX36, see Figure S5 for corresponding controls of expression of hemichannels and AFD thermosensory responses. Error bars denote SEM.